An Efficient Numerical Simulation for Gamma Ray Burst Energy Profiles

Om Kasar and Annika Thomas

Received March 30, 2025
Accepted September 14, 2025
Electronic access September 30, 2025

Gamma-Ray Bursts (GRBs) are one of the most energetic events observed in the universe that can outshine both stars and galaxies alike. GRBs are composed of high-energy photons in the gamma-ray range of the electromagnetic spectrum and propagate at relativistic speeds through the interstellar medium. Due to their extreme speeds, scientists consider the sheer amount of energy that launch the ejecta at speeds nearing the speed of light, or relativistic speeds. These high levels of energy are expended through a beam, which is referred to as the jet of a GRB; these jets are theorized to drive the ejecta at velocities approaching the speed of light. In this work, we observe the dynamics of these jets through a devised and numerically simulated model that dictates energy levels with respect to time and simulate the emission using a Python program for a visual analysis of the model. More specifically, we analyze the jet energy emission (in erg/s) and energy per solid angle analysis for three example GRBs and their properties. We then discuss the outcomes and implications of the results of the simulation, as well as conclusions regarding the experiment. Through our simulation, we show that the jet dynamics produce a theorized "plateau" in energy emission, directly being caused where the GRB turns non-relativistic, transitioning into slower speeds relative to the speed of light. We open source our code to support further research and experimentation, available at https://github.com/Om-Kasar/GRB-Jet-Energy-Model.
Keywords: High Energy Astrophysics, Computational Physics, Numerical Simulation, Relativistic Jets, Gamma Ray Burst

1 Introduction

Gamma Ray Bursts (GRBs) are concentrated beams of photons that occur during especially large cosmic events. GRBs are related to many fundamental areas of astrophysics, including the properties of the surrounding medium and host galaxy, gravitational wave analysis, and the study of cosmic rays [1]. After a GRB's initial emission, it proceeds to travel in the ambient medium at a speed nearing the speed of light, and slows down as a result of a great amount of accumulated mass and energy emission throughout its lifespan in the medium. As a GRB slows down and progresses through the interstellar medium, it slowly transitions to the non-relativistic stage, the stage in which the GRB stops advancing the outside medium at speeds nearing the speed of light. As the GRB experiences a transition to this regime, the dynamics fundamentally change [2], resulting in new dependencies for the central engine, most notably a change from dependence on the initial angle to its observed luminosity profile. For instance, the GRB dynamics transition from a dependency on the emission angle to the total energy emitted of a GRB as it transitions from becoming relativistic to non-relativistic.

As a result of their chaotic outburst being closely associated with cosmic cataclysms [3], scientists hypothesize that the main engine causing the gamma rays, accumulated mass, and other GRB contents (referred to as the ejecta), to move at such speeds is the concept of a jet, a heavily concentrated beam of plasma [4] that occurs at the start of its launch and guides the GRB ejecta through the interstellar environment. The main causes of the jet is by either the merging of a binary system or, more commonly, the collapse of especially massive stars known as collapsars [3]. This hypothesis fails to account for specific dynamics of the jet, such as its energy levels and angular distributions, and remains fairly elusive despite a multitude of studies being done on the topic. Due to our limited understanding of energy emission [5], this work attempts to model an approximation of the energy emission of a given GRB jet throughout its initial prompt emission and its lifetime in the interstellar medium.

The development of multiple technologies, such as the Fermi/LAT telescope [6], has enabled the use of complex GRB afterglow detections to collect vital data of numerous instances of GRB explosions. These technologies directly facilitate many works in the understanding the fundamentals of GRB dynamics. In this work we thank the Swift/BAT GRB catalog in providing the data for conceptual analysis this work [7], as well as the ClassiPyGRB Python library to integrate the catalog with approaches to data analysis [8].

In this work, we begin by explaining the energy emission model in Section 2, including detailed explanation of each component of the model. In Section 3, we simulate the model using a C++ program with a Python interface and compare it to similar models from other works. We then explain the implications and potential flaws that could be improved upon in future studies

© The National High School Journal of Science 2025

in Section 4 and draw conclusions in Section 5 based on our results.

2 Energy Emission Model

In developing this model, we aim to create an accurate and computationally efficient method to track the energy levels of a given GRB jet in a consistent manner. The model leverages the relationship between the initial ejection energy and the decrease in energy levels as the GRB travels through space. For the general model, it's vital to recognize the use and meaning of each ratio, and the magnitude at which it affects the energy of the GRB jet.

2.1 Model Assumptions and Concepts

We begin by providing preliminary explanation of the fundamentals of our energy analysis.

As the jet expands from the central engine, it is expected to collect a large portion of the mass from the external medium at which it is launched in combination with its initial mass gained from the central engine [9]. As the jet steadily sweeps up more mass, the GRB is expected to rapidly decelerate as a result of inertia. Because of this, one of the main factors that directly contributes to the jet's deceleration is the accumulation of mass in the external medium, thus causing a reduction [2] in its energy emission [10]. We define the following values for the mass swept up per solid angle of the GRB according to Wang [11]:

$$M_{sw} = \int \Gamma \rho_{sw} r^2 \, dr \tag{1}$$

where $\rho_{sw} = 4\rho_0\Gamma$ and $\rho_0 \propto r^{-k}$ (k is the power-law index), in accordance with the shock jump condition as seen by Wang [11] and Uhm [12]. The radial integrated value as a function of time will be evaluated in combination with total ejecta mass, defined as the radial integrated value plus the initial mass per solid angle of the GRB. This gives us the following:

$$M_{ej} = M_{sw} + \frac{M_0}{\Omega_0} \tag{2}$$

where M_0 is the initial mass of the GRB and Ω_0 is the initial solid angle of the GRB. In addition, the initial mass of the GRB will be calculated with the following relationship mentioned by Sari [13]:

$$E_0 = M_0 \Gamma_0 c^2 \tag{3}$$

in which E_0 is the initial ejection energy of the GRB.

Furthermore, we assume an energy model in which the energy level dependencies change after the GRB advances through the medium at times $t \geq t_{NR}$, or the times at which the GRB becomes non-relativistic. t_{NR} is defined as the following according to vanEerten's conjecture on GRB propagation

$$t_{NR} = 1100 \left(\frac{E_{\mathrm{iso},0}}{10^{53} n_0} \right)^{1/3} \text{ days} \tag{4}$$

where the $E_{\mathrm{iso},0}$ is the initial isotropic equivalent energy of the GRB, and n_0 is the external medium density in which the GRB is launched. We note that the expression for t_{NR} is in days [2].

The model utilizes a piecewise approximation of the Lorentz factor during a GRB's propagation, where the Lorentz factor is constant until the threshold t = t_{dec}, or the time of rapid deceleration after the GRB's initial outburst, as suggested by Figure 1. We define the approximation to be the following expression in accordance to Uhm's findings [14] on GRB afterglow speeds:

$$\Gamma \approx \begin{cases} \Gamma_0, & 0 \leq t \leq t_{dec} \\ \Gamma_0 \left(\frac{t_{dec}}{t} \right), & t > t_{dec} \end{cases} \tag{5}$$

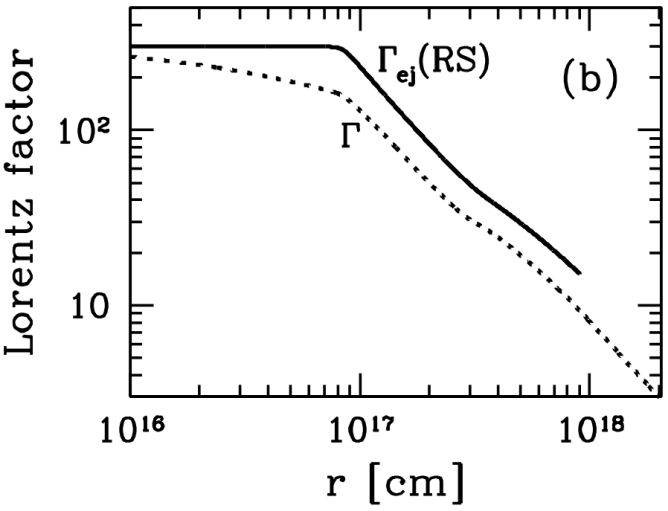

Fig. 1 A GRB afterglow analysis model, detailing the approximate Lorentz factor with respect to radial displacement from the central engine. As shown, the Lorentz factor becomes constant until the $r = 10^{17} cm$ threshold, suggesting a constant Lorentz factor approximation until some drop-off, which may be defined as some time nearing t = t_{dec}. Adapted from Uhm [12].

We utilize this model in order to suggest the same speed throughout the interval [0.01, t_{dec}] and then a sudden drop in velocity after the t_{dec} threshold, to align with Uhm's findings [14] on decreasing Lorentz factors in afterglow propagation.

Lastly, the jet energy levels before t_{NR} depend on the Lorentz factor Γ and ejection angle θ of the GRB. After the t = t_{NR} threshold, the GRB becomes dependent on the radius r from the central engine as well as the total ejection energy emission from luminosity E_{ej} [2]. These parameters will be represented

© The National High School Journal of Science 2025

as decreasing ratios, since the energy decreases as the GRB progresses through the medium.

2.2 Jet Energy Model

Following these assumptions, we now derive the approximate jet energy model. We delve into the possible energy emission, logic behind each component, and its implications on jet energy emission as a whole.

Firstly, we propose the model as a sudden decrease in kinetic and luminous energies shortly after a given GRB's observation, namely at t_{dec}, in which energy levels suddenly drop. Furthermore, a multitude of afterglow simulations and observations noted a sudden plateau in afterglow observation as a result of the theorized "energy reservoir"[15] as the GRB propagates through the medium (observed in Figure 2). We encapsulate these observations through a decreasing reciprocal function, where the value asymptotically approaches some arbitrary horizontal asymptote (say, 10^{45} erg) and produces a "plateau" in overall jet ejection energy. Therefore, in the relativistic stage, we define the expression and scale factor for energy emission (denoted as $dE_{j,R}/dt$ and α, respectively) after our analysis as:

$$\frac{dE_{j,R}}{dt} = E_0 \cdot \left[t \left(1 + \left(\frac{t}{t_{dec}} \right)^{\alpha(t)} \right) \right]^{-1} \tag{6}$$

To detail these dependencies in our model, we define α as:

$$\alpha = \left[\left(\frac{M_{ej}}{M_{sw}} \right)^{0.25} \left(\frac{\Gamma}{\Gamma_0} \right)^{0.5} \left(\frac{\theta_0}{\theta} \right)^{0.5} \right]^{0.5} \tag{7}$$

We include the ratio M_{ej}/M_{sw}, since it elaborates on the dependence of the swept-up mass pattern of the GRB jet, which is thought to cause the deceleration of the GRB with the accumulated mass during its propagation as a result of inertia and conservation of momentum[16]. We set this dependency as a ratio of the total ejecta mass and the swept-up mass to analyze the factor of change in the GRB's mass profile to suggest the change in GRB dynamics with respect to the mass.

The ratio Γ/Γ_0 reflects the dependence on both the Lorentz factor and the initial Lorentz factor on the theoretical kinetic energy emissions of the GRB jet[17]. The Lorentz factor Γ is expected to experience a rapid decrease as it progresses through the medium because the mass is swept by the GRB jet, causing a decrease in the kinetic energy of the ejecta in the interstellar medium.

The component θ_0/θ of our model represents a relationship in which the jet energy directly correlates with the ejection angle compared to its initial launch angle, θ_0, before the time t = t_{NR}, according to vanEerten[2]. The desired output will be similar to a decreasing pattern for the typical GRB explosion. Since $\theta(t)$ is inversely proportional to θ_0, this gives us a decreasing pattern in the observed emission angle that is thought to further decelerate the concentrated ejecta in the medium.

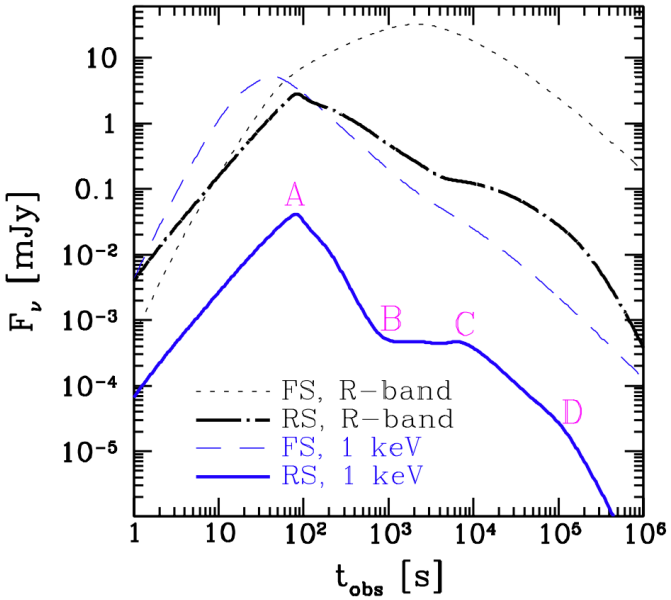

Fig. 2 A representation of the flux density (mJy) from a proposed GRB afterglow model. Represents a theorized "plateau" in observed flux over the interval $[10^3, 10^4]$. Adapted from Uhm[12].

After analyzing the jet energy emission in the relativistic stage, we now present the non - relativistic dynamics of GRB jets. To extend upon the aforementioned plateau, we utilize an exponential decrease in energy in order to elongate the observed plateau and propose a decrease in energy beyond the asymptote in times t_{NR} and beyond. The expression and scale factor, denoted as $\frac{dE_{j,NR}}{dt}$ and β, respectively, can be defined as the following:

$$\frac{dE_{j,NR}}{dt} = \left. \frac{dE_{j,R}}{dt} \right|_{t_{NR}} \cdot \exp(-\beta\,(t - t_{NR})) \tag{8}$$

in which β is:

$$\beta = \left(\frac{r_{NR}}{r} \cdot \frac{E_0}{E_{ej}} \cdot \left(\frac{M_{ej}}{M_{sw}} \right)^{0.25} \right) \tag{9}$$

E_{ej} is defined as the integral of a given light curve of a GRB, given as the following[4,18]:

$$E_{ej}(t) = \frac{\theta(t)^2}{2} \int_{0.01}^{t} L_v(x)\,dx \tag{10}$$

where $L_v(t)$ is the light curve of the GRB and E_{iso} is the isotropic equivalent energy of the light curve. We employ this dependency as a result of the patterns from many Swift/BAT GRB light curves and their tendency to portray a decreasing pattern of luminous energy emission shortly after their violent outburst.

After further analysis of GRB light curves from the Swift/BAT catalog, we point out that, as $t \to \infty$, the ejection energy has negligible changes as a result of the continued sharp decrease of its energy levels[19] from t = t_{dec} and t = t_{NR} thresholds. Therefore, for simplicity, we define the following limit for an approximate expression for $E_{ej}(t)$ in the analyzed computational model to encapsulate the luminous energies of the GRB:

$$\lim_{t\to\infty} E_{ej}(t) \approx E_0 + 1.5 \times 10^{50} \tag{11}$$

We note that the function is directly proportional to $dE_{j,R}/dt(t_{NR})$ in order to ensure a continuous function over the interval (0, t]. This condition is necessary in order to derive the energy per solid angle parametric function, discussed later on in this paper.

The relationship $r_{NR}/r(t)$ signifies the dependency of the radial distance from the central engine after the GRB is in the non-relativistic stage, which is thought to be an indicator of many aspects of GRB energy levels[20]. As the increase in radius from its entity at which the GRB becomes non-relativistic (denoted as r_{NR}, or r(t_{NR})) becomes more significant, the ratio suggests a desired decreasing relationship in radius as a result[21].

The dependency $\frac{E_0}{E_{ej}(t)}$ demonstrates how the observed ejection energy is the dominant factor in the overall dynamics of the jet after passing the t_{NR} threshold[22]. Since the approximate value for overall ejection energy heavily decreases after the main energy emission, we approximate the observed ejection energy independent to the initial energy emitted as $1.5 \cdot 10^{50}$ for a standard GRB.

Finally, we consider the mass profile of our model due to the inertial effect mentioned earlier. We believe that this mass component will continue to create an impact on GRB energy profiling because of a noticeable accumulation of mass even after the t_{NR} threshold.

Composing each component of the equation yields the approximate derivation of the jet energy model (denoted as dE_j/dt) with respect to time. We use a piecewise structure for our model to denote the desired plateau behavior observed in Figure 2, seen as:

$$\frac{dE_j}{dt} = \begin{cases} \dfrac{dE_{j,R}}{dt}(t), & 0 \le t \le t_{NR} \\ \dfrac{dE_{j,NR}}{dt}(t), & t > t_{NR} \end{cases} \tag{12}$$

The energy of the jet model in the relativistic and non-relativistic time ranges can then be represented as the following:

$$\frac{dE_j}{dt}(t) = \begin{cases} E_0 \left[t \left(1 + \left(\frac{t}{t_{dec}} \right)^{\alpha(t)} \right) \right]^{-1}, & 0 \le t \le t_{NR} \\ \left. \dfrac{dE_{j,R}}{dt} \right|_{t_{NR}} \exp(-\beta(t)\,(t - t_{NR})), & t \ge t_{NR} \end{cases} \tag{13}$$

3 Experimentation

We now discuss the experiments used for energy analysis, including the simulation setup as well as our results from numerical simulations. We elaborate on the general experimentation process and possible implications of the numerical simulation in this section as a whole.

3.1 Simulation Setup

For the numerical simulation, our computer's specifications involve an RTX 4060 GPU, an 12th generation Intel CPU, and 16 gigabytes of RAM. We use Python in order to provide a wrapper for the C++ system to interface with the user. We store constants and experiment configurations into a .yaml file for calculations through the Parameters.yaml file and the dynamically constructed CalculatedParameters.yaml file, where the values are created as a result of dependencies located in the Parameters.yaml file. Detailed instructions can be found at the GitHub repository. We then compare 3 sample GRBs' (narrow, medial, and wide GRBs, respectively) properties and jet expansions. We discuss their implications (refer to Table 1 and Table 2), and demonstrate their modeled energy emissions in comparison to one another.

Next, we use C++ in our program for general computational efficiency for each function. After the .yaml files have defined the experimental constants and parameters, we reference the files' parameters in a structure function in the source code, and define them globally for experimentation in the main.cpp file. We then utilize the pybind11 package to compile the C++ program into a .pyd file in order interface with the C++ module in Python. All the ratios involved, including the mass, Lorentz factor, and ejection angle ratios, are included in the package for individual testing if needed.

We evaluate the model by displaying the numerical simulation results through the matplotlib library. We investigate the shapes at which the GRB graphs dE_j/dt change with respect to time for the three GRBs. In addition, we also perform energy per solid angle analysis in order to compare the data with other energy per solid angle models by by parameterizing θ and $dE_j/d\Omega$ for analysis using a similar process.

In the following, we derive the energy per solid angle function, with respect to time. The equations for energy per solid angle (denoted as $dE_j/d\Omega(t)$ or $\varepsilon(t)$) are given by the following:

$$\frac{dE_j}{d\Omega} = \frac{dE_j}{dt} \cdot \frac{dt}{d\Omega} \tag{14}$$

According to Salafia[4] energy per solid angle equates to approximately the initial luminous energy emitted before the relativistic threshold. Therefore, dt/dΩ must then be defined as:

$$\frac{dt}{d\Omega} = \frac{E_0}{dE_{j,R}/dt} = t\left(1 + \left(\frac{t}{t_{dec}} \right)^{\alpha(t)} \right) \tag{15}$$

© The National High School Journal of Science 2025

Table 1 Experiment Configurations for each GRB [Narrow (1, 2), Medial (3, 4), and Long (5, 6, 7)] (Parameters.yaml files)

Parameter	GRB_1	GRB_2	GRB_3	GRB_4	GRB_5	GRB_6	GRB_7
t_{dec} (s)	10	12	15	25	50	70	100
E_0 (erg)	$5.00*10^{51}$	$9.00*10^{51}$	$2.5*10^{52}$	$10^{53}/4\pi$	$8.00*10^{52}$	10^{53}	$2.00*10^{53}$
A (cm)	10^5	$3.5*10^5$	$7.5*10^5$	$4.5*10^6$	$6*10^6$	$8*10^6$	10^7
k	2.2	2	1.7	1.3	1.27	1.22	1.2
n_0 (cm^{-3})	0.01	0.35	0.75	1	1.15	1.35	1.5
θ_0 (rad)	0.05	0.2	0.45	0.7	0.72	0.77	0.8

Using this identity, we can derive the first component of the energy per solid angle model, yielding:

$$\varepsilon_1(t) = E_0 \cdot \left[t \left(1 + \left(\frac{t}{t_{dec}} \right)^{\alpha(t)} \right) \right]^{-1} \cdot \frac{dt}{d\Omega} = E_0 \qquad (16)$$

We can now define energy per solid angle as the following parametric by dividing both parts of the jet energy emission function, giving us:

$$\varepsilon(t) = \begin{cases} E_0, & 0 \le t \le t_{NR} \\ E_0 \cdot \exp\left(-\beta(t) \cdot (t - t_{NR})\right) \cdot \frac{dt}{d\Omega}, & t \ge t_{NR} \end{cases} \qquad (17)$$

3.2 Results

In this section, we now discuss the operation of the computational model, its results, and its implications on jet energy emission as a whole.

For the model, we first input each requested value into the Parameters.yaml file. The experiment configurations are seen in Table 1. We then run the parameters.py file in order dynamically create the CalculatedParameters.py file, which can be seen in Table 2. These experiment configurations will then be processed through the "burstConfigs" alias in the experimental Python files in order to output a numerically simulated graph through the matplotlib Python library.

As seen in Figure 3, the jet emission model somewhat agrees with our hypothetical image of GRB jets. We include the plateau after the t = t_{NR} threshold in order to align with our afterglow analysis. Each simulated GRB represents some form of the theorized plateau in energy emission, as suggested by Figure 1. In addition, as hypothesized, the fundamental dynamics of each GRB jet changes after passing the t = t_{NR} threshold for each GRB.

However, we also observe sharp turns in the model, as shown in the results from GRB_1, GRB_2, and GRB_3. The energy emission model includes these sharp turn as likely as a result of sudden conversion of other forms of energy (e.g. luminosity) or a sudden interaction with a dense medium[23]. Being a narrow GRB with less mass, the jet could have accumulated more mass

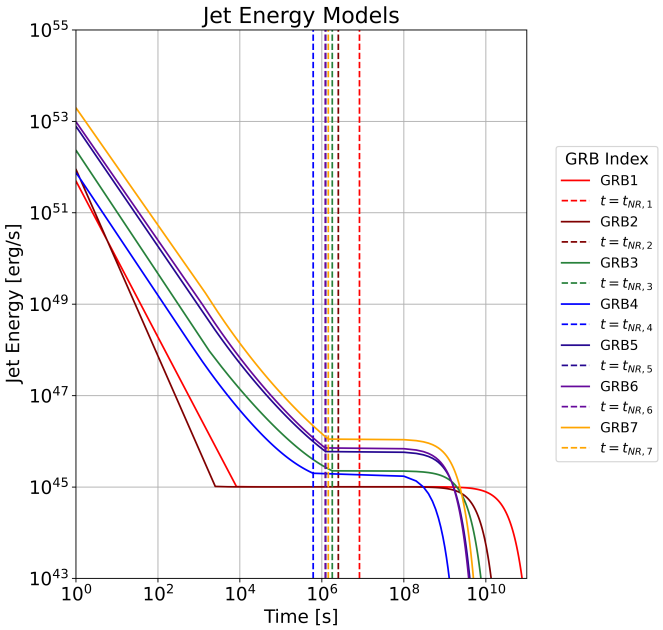

Fig. 3 A numerically simulated graph for dE_j/dt using the approximate jet energy emission model. Burst configuration parameters for each simulated GRB are given in Table 1 and Table 2. Dotted lines represent times in which t = t_{NR} for the narrow, medial, and wide GRBs, denoted with a 1-7 as such with corresponding colors for their respective GRBs. Model error estimates include an approximate margins of $\pm 10^3$ for each analyzed data point in our curves.

and rapidly decelerated through an especially dense medium in order for the plateau phase of its emission much earlier than the other GRBs. However, this hypothesis fails to account for the extended length of the plateau for GRB_1; the jet is expected to accumulate more mass as it propagates through the medium, causing the jet to move slower and exert more energy with a surefire decrease in ejection energy rather than a standard plateau.

Alternatively, we believe that a more plausible explanation for these sharp turns involves the energy reservoir[24]; we believe that these turns result in the narrow GRB's tendency to transition towards their energy reservoir at an increasingly sudden

Table 2 Dynamically Created Configurations for each GRB (CalculatedParameters.yaml files)

Parameter	GRB_1	GRB_2	GRB_3	GRB_4	GRB_5	GRB_6	GRB_7
$E_{iso,0}(erg)$	$8.00*10^{53}$	$4.45*10^{53}$	$2.47*10^{53}$	$3.25*10^{52}$	$3.09*10^{53}$	$3.37*10^{53}$	$6.25*10^{53}$
Γ_0	793.5	474.2	343	212	212.9	186	173.4
M_0 (g)	$1.40*10^{27}$	$2.11*10^{28}$	$8.11*10^{28}$	$4.18*10^{28}$	$4.18*10^{29}$	$6.00*10^{29}$	$1.28*10^{30}$
$t_{NR}(s)$	$8.28*10^{6}$	$2.51*10^{6}$	$1.33*10^{6}$	$6.13*10^{6}$	$1.23*10^{6}$	$1.21*10^{6}$	$1.44*10^{6}$
r_{NR} (cm)	$1.37*10^{29}$	$1.27*10^{28}$	$2.64*10^{17}$	$7.52*10^{31}$	$3.07*10^{32}$	$2.93*10^{32}$	$2.06*10^{29}$

rate during its propagation, which is especially emphasized in Kumar's study [25]. We attribute this theory to a more physically significant explanation of these sharp turns because many studies have alluded to energy-reservoir transitions in narrow and medial GRB's, which are yet to be answered as of now, as seen in Frail's [26] and Panaitescu's [27] works.

A nearly instantaneous change in the jet's internal energy reservoir could also explain the relatively abrupt plateau of GRB_1 and GRB_2. Through potential interactions with the reverse shock during its growth or other internal processes, the GRBs may have instantly dissipated some of its energy in the process of its expansion [28]. This hypothesis could also explain the broad, constant emission of the medial GRBs' graphs, suggesting a negligible difference in energy emission. This could also apply to the sharp turn seen at GRB_5, GRB_6, and GRB_7, but at a much shorter scale throughout its propagation in the medium overall.

We also recognize that, in Figure 3, the GRBs experience an accelerated linear decrease after its initial ejection energy at times nearing t = 10^1 s. This rapid decrease shortly after each GRBs' emission agrees with the conventional understanding of GRBs, in which GRB energy emission decreases from 1-100 seconds after the initial burst emission in the prompt phase [16].

Lastly, we discuss the end behavior of each GRB after its plateau phase in Figure 3. We see that these graphs align with conventional understanding of GRBs; the graphs reveal a constant energy per solid angle profile until it reaches the $\theta = \theta_{NR}$ threshold. We observe an especially heavy decrease over the timescale $\sim t \gg t_{NR}$ in order to account for the increased ejecta density and mass accumulation over the large time period [29]. In combination with the general spreading of the GRB as a result of forward shock expansion, this conjecture agrees with the behavior of many GRBs analyzed in previous studies [24,25].

We now elaborate on the extent of the energy per solid angle analysis. As seen in Figure 4, the energy per solid angle appears to be constant, with a immediate, exponential drop off at θ values around $\sim \Delta\theta = 10^2 - 10^3$. This behavior somewhat aligns with the standard understanding of GRBs. As each GRB traverses the ambient medium, the GRBs are thought to retain its' conical shape before transitioning to the non-relativistic regime, as well as a minimal change in ejection angle from the jet axis [30]. Therefore, we justify the constant energy per solid angle at the start of the energy emission.

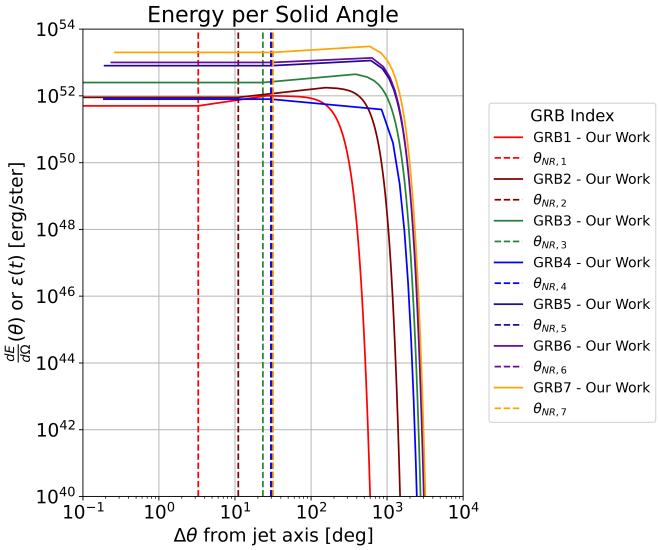

Fig. 4 A numerically simulated graph for $\frac{dE_j}{d\Omega}(t)\,(\varepsilon(t))$ using the approximate energy per solid angle model. The parametric equation for $\varepsilon(t)$ is given in Eq. 17. Simulated burst configurations are given in Tables 1 and 2. Dotted lines represent times in which $\theta = \theta_{NR}$ for the narrow, medial, and wide GRBs, denoted as a number from 1-7 as such with corresponding colors in the legend. Error predictions include values nearing an average of $\pm 10^4$ for each data point in each energy per solid angle curve.

However, this hypothesis does not account for a crucial factor in the profile of energy per solid angle, being the excessive elongation of the energy per solid angle ratio during the interval $\Delta\theta < \theta_{NR}$. This could be due to the constant relationship occurring as a result of minimal changes in angle from the jet axis before the $\theta = \theta_{NR}$ threshold. Therefore, we propose that the model has a substantial decrease in energy per solid angle only after a noticeable change in θ in jet dynamics from its initial angle [31], namely at the θ_{NR} threshold.

The energy per solid angle drop-off is accurate to the average illustration of GRB energy emission as a whole. The steep drop-off appears to be relevant to the general ejection energy after the $\theta = \theta_{NR}$ threshold. The simulated model suggests that, as each GRB becomes non-relativistic, the energy per solid

© The National High School Journal of Science 2025

angle function experiences a great decrease in energy in proportion to the general energy profile dE_j/dt [32]. This conclusion agrees with the general idea of the model, in the sense that a rapid decrease in ejecta energy occurs mainly after the GRB becomes non-relativistic [24], thus yielding accurate models to the jet emission patterns of GRBs.

4 Discussion

4.1 Parameter Sensitivity Analysis and Observational Uncertainties

We now conduct a brief parameter sensitivity analysis for our model to analyze the effects of each parameter usage. For our sensitivity analysis, we run multiple instances of our program with GRB_4 configurations from Tables 1 and 2 and vary the values of the deceleration time t_{dec}, initial energy E_0, density constant A, and initial angle θ_0 to observe the changes in our jet energy curve. We then assess what these changes suggest about the GRB's propagation in the interstellar medium.

With the t_{dec} parameter, we observe a surprising pattern after input values ranging from 10 - 100 s; the decrease in energy emission before the t_{NR} phase appears to alleviate the harsh transition into the plateau phase before the t_{NR} threshold with higher values of t_{NR}. A plausible hypothesis that supports this behavior could be as a result of the GRB's noticeable dependencies after its ultra-relativistic state before the t_{dec} threshold, as seen in a previous study by Sultana [29].

We now analyze the changes in the jet energy curves through various changes in the density [12] proportionality constant A of the GRB ejecta, ranging from $10^4 - 10^8$ cm. As the values of A increases, we observe a GRB energy curve that gives a smoother transition to the energy reservoir state, similar to that of t_{dec}. We believe a main driver for this trend is the increase in the mass ratio of our model as a result of an increased GRB ejecta density, causing our curves to have an increased exponential value for every t during the GRB's propagation.

Finally, we now survey values for θ_0 in radians from 0.1 - 0.85 and observe how our GRB_4 energy curve changes. Based on our analysis, we notice surprising artifacts of our energy curves; as θ_0 increases in value, we note an elongated plateau phase as the GRB traverses the medium before the t_{NR} threshold, likely as a result of the increased angular ratio in our model. This shows us that GRB_4's behavior towards the theorized energy reservoir is heavily dependent on higher values of its initial emission angle, which agrees with Zhang's [33] conclusion in his GRB analysis.

4.2 Comparison with Existing Models and Observational Data

We compare our energy per solid angle model with three other models. In addition to the simulation of this GRB and its implications, we also compare and contrast GRB_2's configurations with our model and three models in order to see how our model fares in comparison to them for energy per solid angle analysis.

We discuss comparative data using a standard Gaussian model. The Gaussian model is given by the following equation, adapted from Salafia [4]:

$$\frac{dE}{d\Omega}(\theta) = E_0 \cdot \exp\left(-\frac{\left(\frac{\theta}{\theta_c}\right)^2}{2}\right) \tag{18}$$

We mention that the values for $\theta$is in degrees for the Gaussian model, and where θ_c = 3 and 4.

Along with this we compare our approximate energy per solid angle model to the GRB energy per solid angle collapsar model detailed by Lazzati [34], which elaborates on the relationship $\frac{dE}{d\Omega}(\theta) \propto \theta^{-2}$, given by the following formula:

$$\frac{dE}{d\Omega}(\theta) = \frac{2\sqrt{3}Lr_*}{\pi c}\,\theta^{-2}, \qquad \theta_{j,br} < \theta < \theta_0 \tag{19}$$

It is worth nothing that this model is also dependent on a degree measure, and applies if the values of $\theta$from the jet axis is within the interval $\theta_{j,br}$ (= 1 in the model) and initial angle θ_0. For the comparative model, we also define r, or the radius of the star in the collapsar model, to be equal to 10^9 cm and L to be constant luminosity $1.5 \cdot 10^{50} erg$. With that being said, we now move on to the assessment of the numerically simulated model in comparison to other models.

As shown in Figure 5, the output is relatively consistent with the formulation of our model. Both curves represent a similar relationship with each other, with a plateau present at the start of its formation. However, in comparison to the Gaussian models, the energy per solid angle ratio of our model appears to drop off much earlier in the jet's propagation. Though each curve represents a similar decrease in energy after its drop-off threshold, the elongated energy per solid angle proves to be a further discrepancy in the model. In fact, the standard Gaussian models appear to asymptotically approach the line $\theta = \theta_{NR}$ instead of having a fundamental change in energy emission. For the collapsar model (refer to Equation 19), the model dictates the energy decrease in our model with an approximate linear decrease in energy with respect to θ. The model manages to estimate the drop off pretty well in comparison to our model, and represents a somewhat accurate depiction of an energy per solid angle profile for GRB_2.

Overall, each model appears to somewhat represent the general consensus of our understanding of GRB energy per solid angle analysis. Despite a few discrepancies in their estimation, they are fairly consistent in drop-off and plateau in general ejection energy at large.

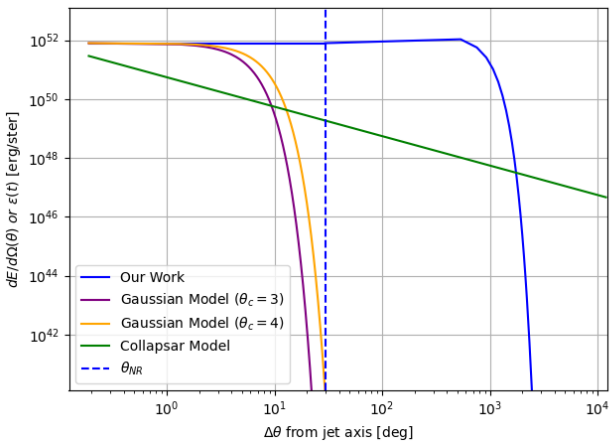

Fig. 5 A numerically simulated graph for GRB_4's $\frac{dE_j}{d\Omega}(\theta)or(\varepsilon(t))$ over a multitude of simulation methods. $\theta = \theta_{NR}$ is labeled as a blue dotted line to represent the threshold value for θ as it passes the non-relativistic threshold. The purple and yellow curves represents the uniform jet model of energy per solid angle between different values of θ_c. The green line represents the collapsar model with a host star radius of $r = 10^9 cm$ and constant luminosity $L \approx 1.5 \cdot 10^{50} erg$ (Refer to Equation 19).

4.3 Model Inconsistencies and Potential Improvements

Though the model appears to be accurate with the general idea of GRB prompt emission, it has some limitations that arise from the assumptions made in our model. We elaborate on how this work could be improved upon in future studies regarding energy emission as well as additional refinements for the model in order to increase its accuracy in modeling jet energy emission and energy per solid angle analysis for GRBs.

The jet energy model includes a broad assumption for the total ejection energy released via luminosity $(E_{ej}(t))$. The model approximates the expression to a constant $\sim E_0 + 1.5 \times 10^{50}$ erg for the sake of simplicity and computational efficiency. However, we caution the use of this ratio in further models to ensure a more accurate representation of the jet energy emission model, since the luminosity does not stay constant throughout its entire duration. We encourage the use of the integral version of the formula for future models in order to have a more accurate profile on the luminosity model as a whole.

In addition, the jet energy graph has many sharp turns, which could either imply a computational error or a different aspect about jet energy emission as a whole. We believe each sharp turn is the direct result of an issue with the computational model, so future models may try to remedy this.

For other GRBs, the plateau in jet energy emission does not necessarily need to be at least at 10^{45} erg. Depending on the burst parameters, future models could calculate a way to calculate this asymptote and apply it accordingly.

We also point out some discrepancies in the energy per solid angle model. In order to improve this model, a shorter horizontal line representing the $\varepsilon(t)$ plateau for any GRB could be the best fit in general energy per solid angle analysis, in accordance to the Gaussian jet energy model.

We also note that the limit used in order to derive the relativistic part $\varepsilon(t)$ is somewhat broad in the overall energy emission of the GRB. The assumption using the limit is could lead to a multitude of inaccuracies seen in Figure 4. A prime example of such behavior possibly due to this limit approximation can be seen through subtle rise in energy per solid angle in each of the GRBs' behaviors. We believe that this discrepancy is an oversight in the calculation for this model. Therefore, we caution further use of the identity used for $\frac{dt}{d\Omega}$ in further models. Instead, we suggest the use of another, alternative expression for $\frac{dt}{d\Omega}$ in order to generate an expression for energy per solid angle.

Based on our analysis, we also detail a few possible observational uncertainties that may occur during the GRB's propagation. We note that the GRB may collide with something during its travels in the medium, which may result in an increased inertial effect and the unexpected change in energy emission for the GRB. In addition, the GRB may experience sudden internal shocks during its initial ultra-relativistic outflow stage[35] and disrupt energy emission patterns in our numerical model. Therefore, we illustrate the need to account for these patterns in energy emission in future works containing our numerical model.

5 Conclusion

In this paper, we discussed the theoretical jet dynamics and jet energy emission in a given GRB's propagation. We developed a reciprocal function and exponential model for mapping out the general energy profile of a GRB's lifespan and observation accordingly by graphing jet energy emission and energy per solid angle analysis through a numerically simulated model in C++ and Python. After discussing the simulation of the model, we construe a few main conclusions regarding the dynamics of GRBs. The results for the energy profiles for each GRB are likely dependent on the energy reservoir that a given GRB as it traverses the medium. The main cause of the plateau behavior in both jet ejection energy and energy per solid angle models alike point to the idea of an energy reservoir and emits a constant energy release, as seen in the simulated models. Even though there are some discrepancies in the conceptualization and calculation of the model, each curve is consistent with other models and concepts. The energy per solid angle analysis, though having a more elongated plateau in its emission, still accurately represented a drop-off similar to that of the discussed energy per solid angle models. As a result of the similar behavior in accordance to other models, we conclude that the jet energy emission appear to be proportional to the ratio of each of the

© The National High School Journal of Science 2025

burst parameters and their function counterparts, represented as decreasing ratios. We encourage future works on the topic to further advance the fundamental understanding of GRBs using these ratios if needed. In addition, the GRB jet has some change in dynamics over its energy profile in order to produce a plateau. In our work, we proposed that this threshold is t = t_{NR} and used that as a basis for all of our analysis. The formula used to calculate t = t_{NR} could be different as a result of elongated constant energy per solid angle emissions in Figure 4 and Figure 5.

This study was facilitated Swift/BAT GRB Catalog and the ClassiPyGRB Python library.

References

1 A. Gomboc, *Contemporary Physics*, 2012, **53**, 339–355.

2 H. J. van Eerten and A. I. MacFadyen, *The Astrophysical Journal*, 2012, **751**, 155.

3 R. Maccary, C. Guidorzi, L. Amati, L. Bazzanini, M. Bulla, A. E. Camisasca, L. Ferro, F. Frontera and A. Tsvetkova, *arXiv preprint*, 2024.

4 O. S. Salafia, G. Ghisellini, A. Pescalli, G. Ghirlanda and F. Nappo, *Monthly Notices of the Royal Astronomical Society*, 2015, **450**, 3549–3558.

5 N. Gupta and B. Zhang, *Monthly Notices of the Royal Astronomical Society: Letters*, 2007.

6 W. B. Atwood, A. A. Abdo, M. Ackermann, W. Althouse, B. Anderson, M. Axelsson, L. Baldini, J. Ballet, D. L. Band, G. Barbiellini *et al.*, *The Astrophysical Journal*, 2009, **697**, 1071–1102.

7 T. Sakamoto, S. D. Barthelmy, L. Barbier, J. R. Cummings, E. E. Fenimore, N. Gehrels, D. Hullinger, H. A. Krimm, C. B. Markwardt, D. M. Palmer *et al.*, *The Astrophysical Journal Supplement Series*, 2008, **175**, 179–190.

8 K. Garcia-Cifuentes, R. L. Becerra and F. De Colle, *Journal of Open Source Software*, 2024, **9**, 5923.

9 J. Granot, *Monthly Notices of the Royal Astronomical Society*, 2011, **421**, 2442–2466.

10 M. K. Bowman, J. P. Leahy and S. S. Komissarov, *Monthly Notices of the Royal Astronomical Society*, 1996, **279**, 899–914.

11 H. Wang, R. G. Dastidar, D. Giannios and P. C. Duffell, *The Astrophysical Journal Supplement Series*, 2024, **273**, 17.

12 Z. L. Uhm, *The Astrophysical Journal*, 2011, **733**, 86.

13 R. Sari, T. Piran and R. Narayan, *The Astrophysical Journal*, 1998, **497**, L17.

14 Z. L. Uhm and A. M. Beloborodov, *Astrophysical Journal Letters*, 2007, **665**, L93.

15 M. G. Dainotti, S. Nagataki, K. Maeda, S. Postnikov and E. Pian, *Astronomy & Astrophysics*, 2017, **600**, A98.

16 T. Piran, *Reviews of Modern Physics*, 2005, **76**, 1143–1210.

17 Y.-F. Liang, B. Zhou, H.-N. He, P. H. T. Tam, Y. Fan and D. Wei, *The Astrophysical Journal*, 2013, **781**, year.

18 R. Gill, M. Kole and J. Granot, *arXiv preprint*, 2021.

19 X.-F. Cao, W.-W. Tan, Y.-W. Yu and Z.-D. Zhang, *arXiv preprint*, 2023.

20 A. J. Van Der Horst, A. Kamble, L. Resmi, R. Wijers, D. Bhattacharya, B. Scheers, E. Rol, R. G. Strom, C. Kouveliotou, T. A. Oosterloo and C. H. Ishwara-Chandra, *arXiv preprint*, 2008.

21 D. M. Wei and T. Lu, *arXiv preprint*, 2000.

22 J.-J. Geng, B. Zhang, A. Kölligan, R. Kuiper and Y.-F. Huang, *The Astrophysical Journal Letters*, 2019, **877**, year.

23 Z.-G. Dai and T. Lu, *The Astrophysical Journal Letters*, 1999, **519**, L155–L158.

24 Y.-F. Huang, L.-J. Gou, Z.-G. Dai and T. Lu, *The Astrophysical Journal*, 2000, **543**, 90.

25 P. Kumar, A. D. Panaitescu and L. Piro, *arXiv preprint*, 2001.

26 D. A. Frail, S. R. Kulkarni, R. Sari, S. G. Djorgovski, J. S. Bloom, T. J. Galama, D. E. Reichart, E. Berger, F. A. Harrison, P. A. Price *et al.*, *The Astrophysical Journal*, 2001, **562**, L55.

27 A. D. Panaitescu and P. Kumar, *The Astrophysical Journal*, 2001, **554**, 667–677.

28 T. Laskar, E. Berger, B. A. Zauderer, R. Margutti, A. M. Soderberg, S. Chakraborti, R. Lunnan, R. Chornock, P. Chandra and A. Ray, *The Astrophysical Journal*, 2013, **776**, 119.

29 J. Sultana, D. Kazanas and A. Mastichiadis, *The Astrophysical Journal*, 2013, **779**, 16.

30 J.-J. Geng, B. Zhang and R. Kuiper, *The Astrophysical Journal*, 2016, **833**, year.

31 J. Granot, P. Kumar and T. Piran, *arXiv preprint*, 2004.

32 D. Guetta, *arXiv preprint*, 2005.

33 B. Zhang and P. Mszros, *The Astrophysical Journal*, 2002, **571**, 876.

34 D. Lazzati and M. C. Begelman, *The Astrophysical Journal*, 2005, **629**, 903–907.

35 S. K. M. Rahaman, J. Granot and P. Beniamini, *Monthly Notices of the Royal Astronomical Society: Letters*, 2023, **528**, L45–L51.

© The National High School Journal of Science 2025